IOPscience iopscience.iop.org

Home Search Collections Journals About Contact us My IOPscience

Group-III nitride quantum heterostructures grown by molecular beam epitaxy

This article has been downloaded from IOPscience. Please scroll down to see the full text article.

2001 J. Phys.: Condens. Matter 13 6945

(http://iopscience.iop.org/0953-8984/13/32/305)

View the table of contents for this issue, or go to the journal homepage for more

Download details:
IP Address: 171.66.16.226
The article was downloaded on 16/05/2010 at 14:04

Please note that terms and conditions apply.

INSTITUTE OF PHYSICS PUBLISHING JOURNAL OF PHYSICS: CONDENSED MATTER

J. Phys.: Condens. Matter **13** (2001) 6945–6960 PII: S0953-8984(01)24816-4

Group-III nitride quantum heterostructures grown by molecular beam epitaxy

Nicolas Grandjean, Benjamin Damilano and Jean Massies

CRHEA–CNRS, rue B Grégory, Sophia Antipolis, 06560 Valbonne, France

Received 14 May 2001
Published 26 July 2001
Online at stacks.iop.org/JPhysCM/13/6945

Abstract

In the present paper, we address a review of group-III nitride quantum wells and quantum dots realized by molecular beam epitaxy (MBE) using ammonia as a nitrogen source. Some important features of the growth of nitrides by MBE using ammonia are pointed out. We also emphasize the role of *in situ* analysis tools such as reflection high-energy electron diffraction. The optical properties of several kinds of quantum heterostructure are presented. They illustrate well the combined effects of polarization fields and carrier localization. Finally, the use of InGaN/GaN QWs in LEDs for white light emission is presented.

1. Introduction

Molecular beam epitaxy (MBE) remains indubitably the technique of choice for growing quantum well (QW) [1–3] and quantum dot (QD) heterostructures [4–7]. This is closely related to the use of reflection high-energy electron diffraction (RHEED) for growth monitoring in real time and precise determination of the alloy composition and the growth rate [8]. Moreover, the latter can be small enough to have a perfect control of the QW thickness with an accuracy better than the molecular monolayer (ML, 1 ML = 2.59 Å in GaN) [9]. Another advantage of MBE concerns the abruptness of the heterointerfaces since the usual growth conditions are very far from equilibrium. In particular, low growth temperatures avoid a strong intermixing at the interfaces.

The weak point of the MBE growth of nitrides was for a long time related to the lack of an efficient nitrogen source. Although the first generation of nitrogen plasma-sources suffered from low growth rates and ionic species, highly detrimental for the material quality, the present sources deliver a sufficient amount of nitrogen active species to grow high-quality GaN above 1 μm h^{-1}. Such characteristics are also achievable using ammonia, which is cracked on the growth surface [10–12].

The realization of well controlled QW structures is of prime importance for the basic study of polarization fields in III–V nitrides. Because of the lattice mismatch between the different binary compounds, the very large piezoelectric constants, the presence of a spontaneous polarization and the growth along a polar axis, the built-in electric field is huge in nitride

heterostructures. Bernardini and coworkers have predicted polarization fields as high as 10 and 15 MV cm^{-1} for GaN/AlN and InN/GaN QWs, respectively [13]. We thus may expect a giant quantum confined Stark effect (QCSE), which has the consequence of red-shifting the QW transition energy [14–16]. Besides this effect, the internal electric field also separates the carriers along the growth axis, leading to a strong reduction of the oscillator strength for wide QWs. Consequently, the radiative lifetime drastically increases, making it easier for the carriers to recombine non-radiatively on dislocations. However, this scenario happens only if the carriers are free to move in the material. Obviously, once they are trapped in deep potential wells they can no longer diffuse toward dislocations. In that case the radiative efficiency is enhanced provided the density of localization centres is much larger than the dislocation density. The use of QDs for increasing the radiative efficiency in defective materials was first demonstrated by Gérard *et al* in the case of the InAs/GaAs system grown on silicon substrates [17]. The high level of performance of group-III nitrides based light emitting diodes and laser diodes, considering the huge density of defects, was ascribed to the formation of In-rich clusters acting as QDs in the InGaN layer [18]. They were observed by transmission electron microscopy (TEM) and explained by InGaN alloy phase separation. More recently, GaN/AlN and InGaN/GaN QDs were fabricated, taking advantage of the Stranski–Krastanov (SK) growth mode transition [4–7]. An increase of the radiative efficiency was also reported for both systems despite the detrimental effect of giant electric fields (more than 5 MV cm^{-1} for GaN/AlN QDs).

In this paper, we report on different kinds of group-III nitride heterostructures. GaN/AlGaN QWs are first discussed in order to emphasize the polarization field effect. GaN/AlN QDs are then presented and their optical properties demonstrate the important role of carrier localization for radiative efficiency. Then, we discuss the growth and the properties of InGaN/GaN QWs, which are governed by both QCSE and localization effects. Finally, InGaN/GaN QWs are used as active layers in LEDs for white light emission.

2. Experiments

GaN, AlN, AlGaN and InGaN layers are grown by MBE on (0001) sapphire or (111) silicon substrates. Double-filament effusion cells are used for Ga and In elements and a cold lips cell is used for Al. The decomposition of NH_3 (50 sccm) on the growth surface provides the nitrogen active species. Details of the growth procedures developed for sapphire and silicon substrates can be found in [12] and [19], respectively. The growth of GaN and AlGaN is carried out at 1–1.5 $\mu m\ h^{-1}$ and 800 °C. AlN is deposited at 0.1–0.3 $\mu m\ h^{-1}$ and 850–900 °C. InGaN growth is carried out at 500–600 °C and 0.05–0.5 $\mu m\ h^{-1}$. In the latter case, the NH_3 flux is increased to 200 sccm for growing InGaN/GaN QWs. The Al composition is deduced from RHEED specular beam intensity oscillations (figure 1). Depending on the growth conditions, the In composition is measured either by RHEED oscillations or high-resolution x-ray diffraction (HRXRD) performed on InGaN/GaN multiple (M) QWs. The PL experiments are carried out using a HeCd laser (325 nm) or a frequency-doubled Ar laser (244 nm).

3. Results and discussion

3.1. GaN/AlGaN QWs

Figure 2 displays a low-temperature (2 K) PL spectrum of a GaN/$Al_{0.08}Ga_{0.92}N$ single (S) QW. The sharp peak at 3.53 eV is ascribed to the QW ground state transition energy while the peak at higher energy corresponds to the barrier emission. The QW PL energy is larger than the

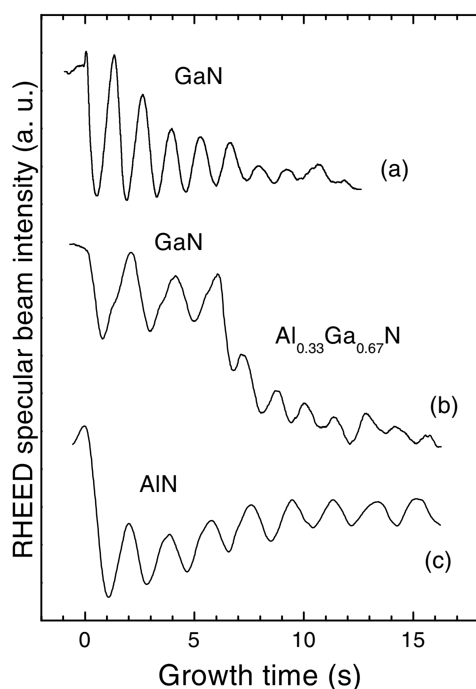

Figure 1. RHEED specular beam intensity oscillations of GaN (a), AlGaN (b) and AlN (c). From such oscillations, precise growth rate and ternary alloy composition can be deduced in real time. One period corresponds to the growth of one molecular monolayer.

GaN band gap due to the carrier quantum confinement associated with the thin well thickness ($L_w = 2$ nm). The full width at half maximum (FWHM) is 9 meV, that indicates smooth interfaces. Obviously, the QW PL peak broadens as the Al composition in the barrier increases. We will see hereafter that there are two main factors contributing to the PL linewidth of nitride based QWs, which is generally much larger than that of QWs based on more conventional materials like III–V arsenides.

Another sample has been grown with a series of QWs of various well thicknesses. The sample structure is four $GaN/Al_{0.13}Ga_{0.8}N$ QWs of width 1, 2, 3 and 4.5 nm separated by a 10 nm thick barrier. The PL spectrum recorded at 10 K is shown in figure 3. The QW PL peaks are clearly resolved with FWHM in the 15–20 meV range. One has to point out that the transition energy of the wider well is lower than the GaN band gap emission (3.478 eV for the A-free exciton in our GaN samples grown on sapphire). The red-shift of the QW transition energy for wider wells is the consequence of a QCSE due to a giant polarization field that builds in wurtzite phase III–V nitride heterostructures. The magnitude of the internal electric field can be easily estimated by fitting the QW transition energy as a function of the well thickness [20]. The QW ground state energy is calculated using simple envelope function calculations in which the electric field has been included. For example, we report in figure 4 the results of these calculations for $GaN/Al_{0.17}Ga_{0.83}N$ QWs. In that case, the QW PL energy variation versus well thickness is accounted for by an electric field of 710 kV cm^{-1}.

This electric field is a consequence of the presence of a macroscopic polarization in the nitride layers. Actually, at the interface between two nitride materials, a monopolar charge appears given by the difference of the total polarization (piezoelectric and spontaneous)

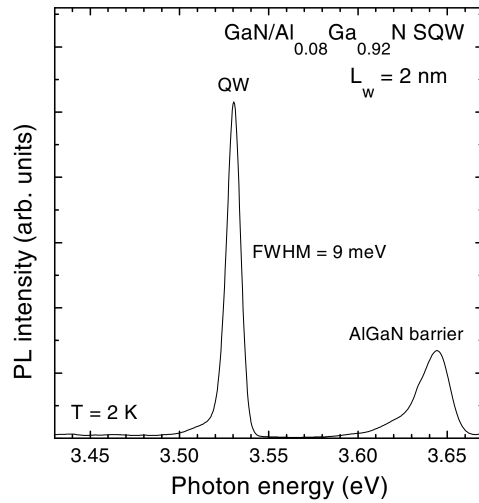

Figure 2. 2 K L spectrum of GaN/$Al_{0.08}Ga_{0.92}N$ SQW grown on sapphire by MBE.

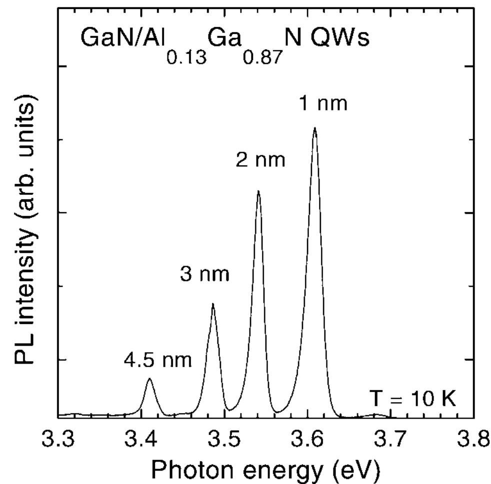

Figure 3. 10 K PL spectrum of a sample that contains four GaN/$Al_{0.13}Ga_{0.87}N$ QWs. The well thicknesses are 1, 2, 3 and 4.5 nm and the $Al_{0.13}Ga_{0.87}N$ barrier thickness is 10 nm.

between the two compounds [13]. The piezoelectric polarization depends on the strain whereas the spontaneous polarization does not. HRXRD performed on our QW samples shows that the AlGaN barriers are pseudomorphically strained onto relaxed GaN buffer layer [20]. Consequently, the piezoelectric effect occurs mainly in the barriers and not in the well. It should be remarked that this situation is opposite to what happens in the GaAs/GaInAs QWs grown along the [111] polar axis. A counterintuitive remark is that the effect of a biaxial compressive strain in GaN wells is the same as that of a biaxial tensile strain in AlGaN barriers (neglecting the deformation potential effects and the slight differences in piezoelectric constants).

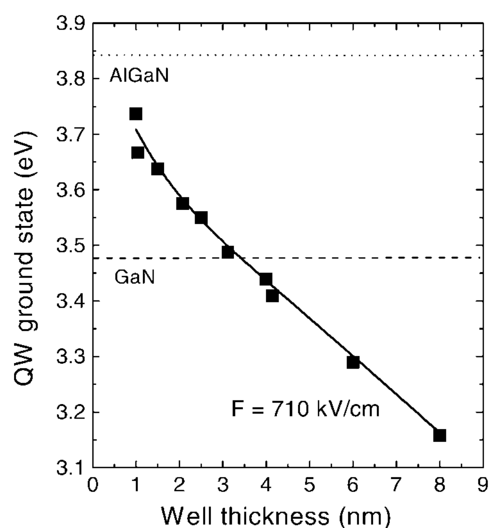

Figure 4. Experimental (closed squares) and calculated transition energies of GaN/$Al_{0.17}Ga_{0.83}N$ QWs (full line).

3.2. GaN/AlN QDs

The manifestation of a giant QCSE is well exemplified in GaN/AlN QDs. They are fabricated taking advantage of the 2.5% lattice-mismatch between GaN and AlN. Above a critical thickness (3 MLs), 3D islands self-form because elastic relaxation at their free edges releases part of the strain-induced elastic energy [21]. However, in ammonia MBE, the 3D islands are not formed by a true SK growth mode regime as observed in plasma MBE [4]. In our case, 3D islands are formed only if a growth interruption without NH_3 flux is performed [5]. The presence of hydrogen or NH_x species adsorbed on the surface may be invoked to explain the hindering of island formation. Either these species reduce the adatom surface diffusion length or they increase the surface free energy, or both. Figure 5 displays RHEED patterns corresponding to the growth procedure we used to form the GaN 3D islands. 5 ML of GaN is deposited onto a relaxed AlN layer. At this stage, the GaN layer is smooth, as attested by the streaky RHEED pattern, and is stable against a growth interruption under NH_3 flux (figure 5(a)). As soon as the NH_3 flux is turned off, the RHEED pattern becomes spotty as the signature of 3D island formation (figure 5(b)). Note that this growth procedure must be carried out within a temperature window (770–820 °C): high enough to allow sufficient mass transport, but not too high to avoid strong decomposition of GaN under vacuum [22]. The formation of 3D islands has been confirmed by atomic force microscopy (AFM) observations (figure 6). An important point concerns the island density, that ranges between 1 and 5×10^{11} cm^{-2}. This is one or two orders of magnitude larger than the dislocation density. This means that most of the QDs, which are simply obtained by AlN capping, are free of defects.

The optical properties of such GaN/AlN QDs have been studied by PL spectroscopy. A giant red-shift of the transition energy due to QCSE is observed as the manifestation inside the dots of a huge built-in electric field along [0001] [13]. The emission energy of the QDs can be tuned over the whole visible spectrum [5]. Figure 7 displays 300 K PL spectra of GaN QDs in AlN matrix grown on (111) silicon substrate. Increasing the dot size, the PL energy maximum red-shifts from 2.8 eV (blue) to 2.1 eV (orange). These energies are far below

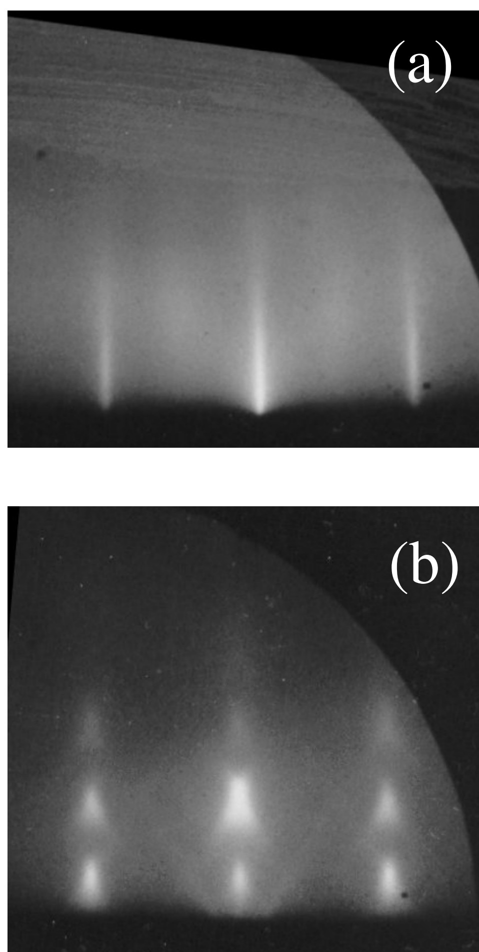

Figure 5. RHEED patterns: (a) 5 MLs of GaN/AlN with NH_3 flux and (b) 5 MLs of GaN/AlN without NH_3 flux.

the band gap of GaN, which forms the dots. Actually, in that case GaN is bi-axially strained onto AlN and the 300 K band gap is about 3.6 eV. Such a low PL energy from the AlN/GaN QDs system is obviously the consequence of a giant QCSE. It should be recalled that theory predicts an electric field as high as 10 MV cm^{-1} in that system. The experimental electric field magnitude can be estimated by plotting the PL energy as a function of the dot height measured by TEM. However, we have to keep in mind that screening of the electric field by free carriers may occur [23]. Therefore, the electric field we measured is underestimated and depends on the excitation power density. With our experimental setup, we deduced a value of 4 MV cm^{-1}, in agreement with data published in the literature for GaN/AlN QDs [4]. As already mentioned, an important consequence of this huge electric field is to strongly decrease the oscillator strength of excitons and thus to increase the radiative lifetime. The observation at room temperature of PL signal from 'red' QDs, for which the QCSE has the stronger effect on the oscillator strength, is an indication that although the radiative lifetime becomes very long, non-radiative recombinations are hindered due to the spatial confinement of carriers. As

an illustration of the role of carrier localization on the PL efficiency, we compare in figure 8 the integrated PL intensity of a GaN/AlN QD system and a GaN epilayer. While the PL intensity of the latter decreases by more than two orders of magnitude, the ratio between 10 and 300 K for the QD sample is only about 2.

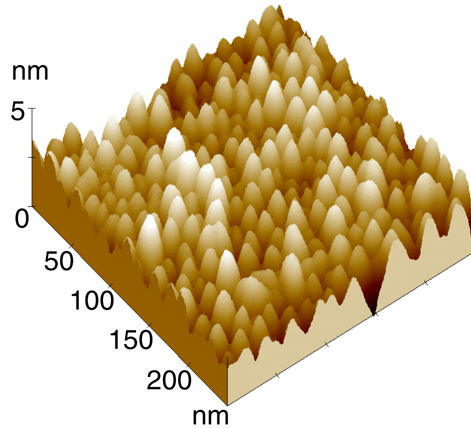

Figure 6. AFM image of uncapped GaN islands.

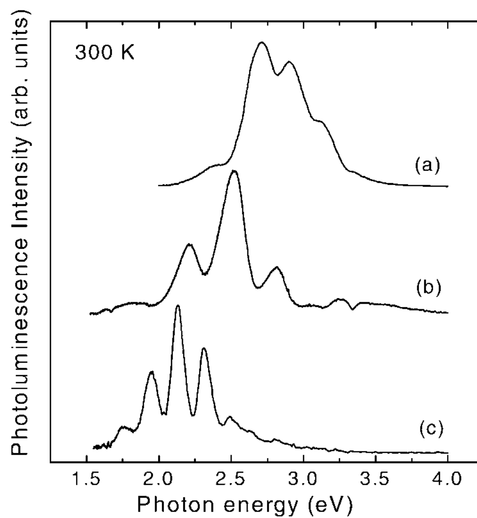

Figure 7. 300 K PL spectra of GaN/AlN QDs grown on (111) silicon substrate. The nominal GaN layer thicknesses are (a) 7, (b) 10 and (c) 12 ML.

3.3. InGaN/GaN QDs

InGaN/GaN QDs are very attractive for optoelectronic device applications such as LEDs since they may produce strong visible luminescence by electrical injection [24]. Note that Narukawa first proposed that InGaN/GaN QDs, formed by InGaN phase separation during MOCVD growth process, are responsible for the high brightness of LEDs [18]. Another way

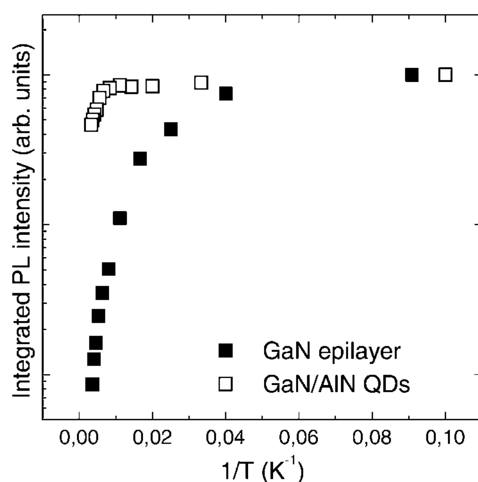

Figure 8. Arrhenius plots of GaN/AlN QDs and GaN epilayer grown on (0001) Al_2O_3.

to fabricate InGaN/GaN QDs is to take advantage of the very high (11%) lattice mismatch between GaN and InN. It is indeed well known that an SK growth mode regime occurs in semiconductors when the lattice mismatch is sufficiently high (generally larger than 1–2%). As already mentioned above in the case of the GaN/AlN material system, the driving force for the 2D–3D transition is the relaxation of the accumulated elastic energy by the 3D island free edges [21, 25]. Actually, 3D islands appear above a critical elastic energy (corresponding to a critical thickness) because of the counteraction of the surface free energy term [26]. The critical In composition was determined by using RHEED intensity oscillations [27]. It should be pointed out that this value depends on the growth conditions, i.e. on the surface free energy, which depends on the V/III ratio, or on the substrate temperature (kinetics limitation). We have measured a critical In composition of 12% for the SK growth mode regime in the InGaN/GaN system (figure 9). Note that a value of 18% was found in plasma-assisted MBE [7]. The critical thickness for 3D island formation is very small, only a few ML (figure 9). The optical properties of $In_{0.15}Ga_{0.85}N$ QDs have been investigated by PL [6]. They exhibit 300 K PL with energy maxima ranging from 3.1 eV to 2.6 eV. The lower energy limit (PL intensity rapidly vanishes in this energy range) is due to QCSE, which once again strongly reduces the oscillator strength. An In composition larger than 15% is needed to get larger wavelength luminescence.

3.4. InGaN/GaN QWs

In order to increase the In composition, we have drastically changed the growth conditions. In particular we have increased the V/III ratio by supplying a larger NH_3 flux. This allows us to push up the In composition to 20%. However, we observed a change in the growth mode, as shown in figure 10 where are reported specular beam RHEED intensity oscillations. For an NH_3 flow of 50 sccm, the growth mode of $In_{0.13}Ga_{0.87}N$ on GaN undergoes a 2D–3D transition after a few ML [27]. This critical thickness is slightly delayed when increasing the NH_3 flow to 100 sccm. When using a larger NH_3 flow (200 sccm), the 2D–3D growth mode transition is no longer observed. This behaviour can be ascribed to a surfactant effect of hydrogen and/or NH_x radicals, as previously discussed for the GaN/AlN QD formation. The reason for the suppression of the 2D–3D growth mode transition could be an increase of the

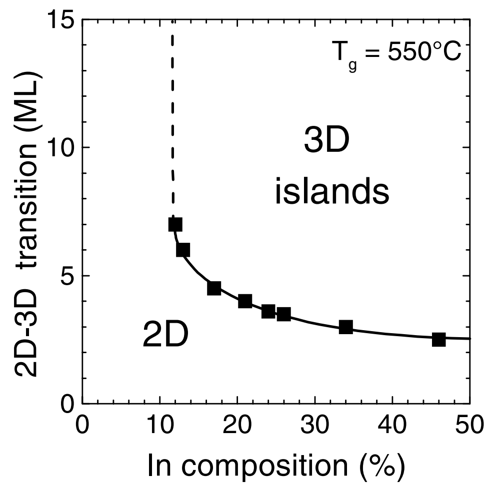

Figure 9. Critical thickness for the 2D–3D growth mode transition during the growth of InGaN/GaN.

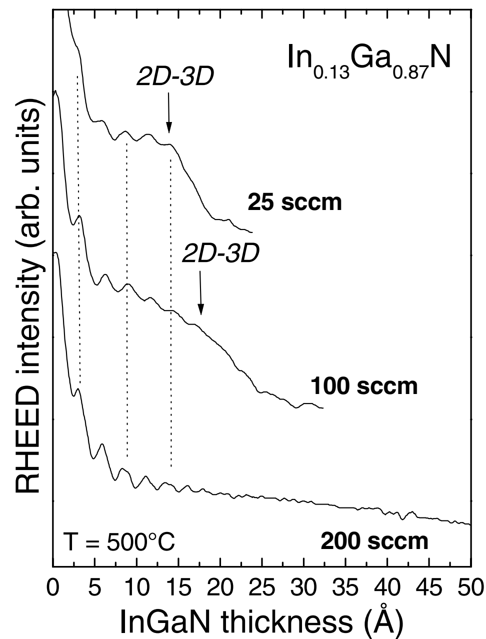

Figure 10. RHEED intensity oscillations showing the delay of the 2D–3D growth mode transition when the NH_3 flux is increased.

surface free energy of the (0001) plane induced by the presence of hydrogen [28] produced by the decomposition of NH_3. We have thus grown $In_{0.2}Ga_{0.8}N/GaN$ QWs with a large amount of NH_3.

Figure 11 displays a HRXRD spectrum recorded around the GaN(0002) Bragg reflection of five periods of an InGaN/GaN QW. The fit of the experimental curve allows one to measure

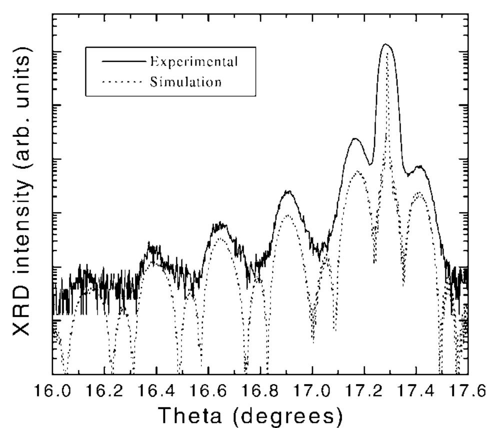

Figure 11. XRD spectrum of a 5 × $In_{0.2}Ga_{0.8}N$(4 nm)/GaN(14 nm) MQW.

Figure 12. TEM image of a 3.5 nm thick $In_{0.2}Ga_{0.8}N$/GaN QW.

an In composition of 20%, and InGaN and GaN thicknesses of 4 nm and 14 nm, respectively. The numerous satellite peaks, up to the fourth order fringe, indicate good interface quality and reproducibility of the InGaN/GaN QW growth sequence. TEM images in cross section confirm the sharpness of the InGaN/GaN interfaces (figure 12). One can clearly see in figure 12 the InGaN/GaN QW, which displays a quite good well thickness homogeneity. Note also that there is no evidence of InGaN alloy phase separation. However, one cannot discard slight In composition fluctuation in the well.

We report in figure 13 the low-temperature PL spectra of $In_{0.2}Ga_{0.8}N/GaN$ QWs with thickness varying from 3 nm to 5.5 nm. The PL energies cover the whole visible spectrum with a lower energy limit below 2 eV. The band gap of the $In_{0.2}Ga_{0.8}N$ being 2.7 eV [29], the QW transition energies are thus red-shifted by giant QCSE. The magnitude of the electric field, deduced from the fit of the PL energies against well width, is indeed very large since it reaches 2.5 MV cm^{-1}. Let us now consider the PL linewidths that range between 70 and 90 meV whatever the PL energy. They are actually rather low values owing to the numerous factors that may contribute to the PL broadening in the InGaN/GaN QW system. The first reason for broadening is related to the strong band gap bowing parameter of the InGaN alloy [29, 30]. It indeed produces a band gap variation of ~80 meV when the In composition fluctuates by ±1% around the 20% average value. Another origin of the PL broadening comes from the giant QCSE. Taking into account an internal electric field of 2.5 MV cm^{-1}, a well thickness fluctuation of ±1 ML involves a PL energy variation of 130 meV. Moreover, ±1% of In composition induces an electric field variation of about ±125 kV cm^{-1}, which leads in turn to an energy variation of 50 meV. All these broadening factors taken together may produce a PL energy variation of 260 meV for only ±1% In composition and ±1 ML well

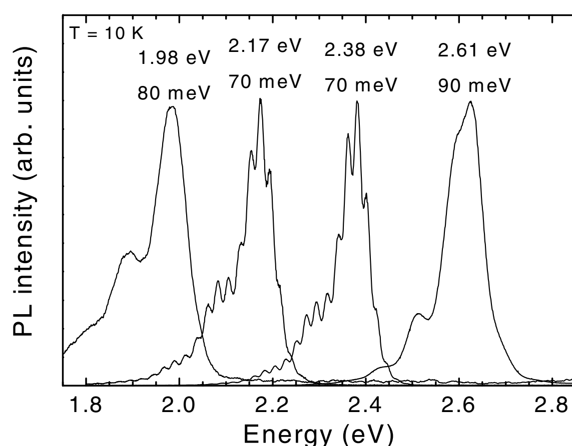

Figure 13. PL spectra of $In_{0.2}Ga_{0.8}N$/GaN QWs of various thicknesses: 3, 3.5, 4.5 and 5.5 nm from blue to red.

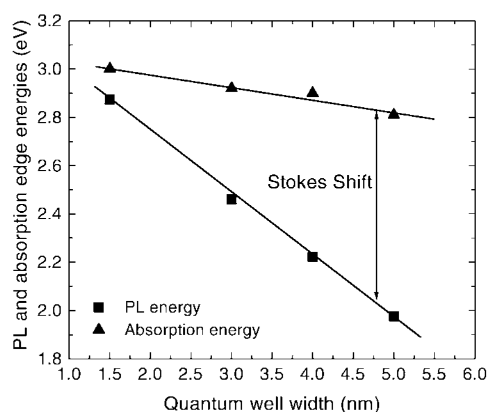

Figure 14. PL and absorption edge energies measured at low temperature (10 and 0.35 K, respectively) on $In_{0.2}Ga_{0.8}N$/GaN QW samples.

thickness fluctuations. The experimental PL linewidths lower than 100 meV at 10 K (150 meV at 300 K) are thus a strong indication that both the In composition and the well thickness fluctuations are not very large. Nevertheless, we will see below that carrier localization in potential fluctuations are necessary for explaining the optical properties, in particular the high PL efficiency of InGaN/GaN QWs compared to GaN/AlGaN QWs.

Another consequence of the huge built-in electric field is the large Stokes shift between the PL peak and the absorption edge [31]. As can be seen in figure 14, the Stokes shift increases with the well thickness. For wide wells, the separation of carriers reduces the absorption of the ground state to nearly zero while it is responsible for PL emission. Actually, the absorption occurs mainly via the excited states at higher energies. In the present samples, the Stokes shift is very large and reaches 830 meV for InGaN/GaN QWs emitting at 2 eV. Although the experienced Stokes shift can be explained by QCSE, one has to consider another contribution, which is the carrier localization. With the aim of getting evidence for such an effect, temperature dependent PL experiments have been carried out on InGaN/GaN QWs. The

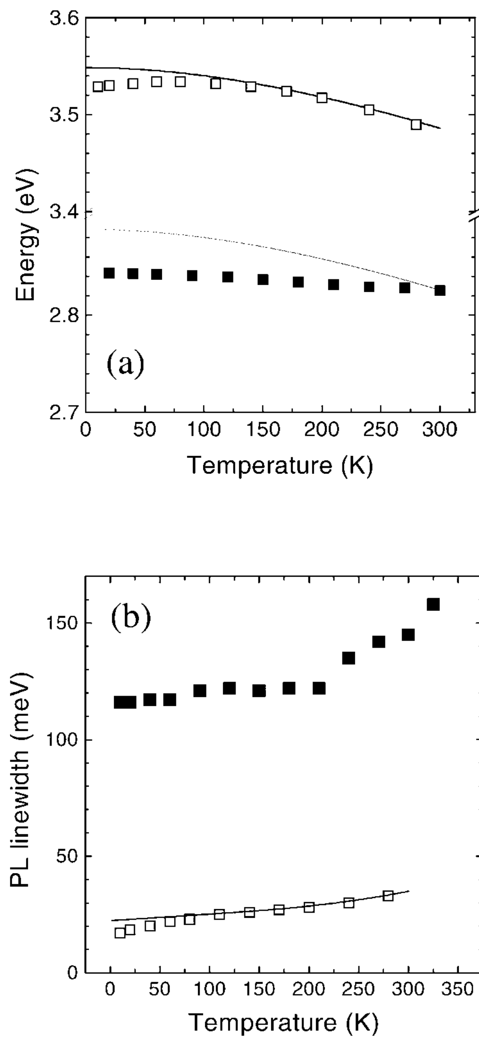

Figure 15. (a) PL energy of a GaN/AlGaN QW (open squares) and an InGaN/GaN QW (closed squares). Full lines correspond to Varshni's equation for band gap variation. (b) PL linewidth of the same samples.

transition from free excitons to localized excitons can be exemplified through the PL linewidth and energy variations. These data are reported in figure 15 for an $In_{0.2}Ga_{0.8}N/GaN$ QW (closed squares) and a GaN/AlGaN QW (open squares). Regarding the PL energy behaviour between 300 K and 100 K, the GaN/AlGaN QW follows the standard band gap variation described by the semi-empirical Varshni equation (figure 15(a)). This corresponds to the free exciton regime. Below 100 K, the PL energies are lower than those expected from Varshni's equation. This is the signature of the exciton localization. One can estimate the localization energy from the difference of the experimental PL energy at low temperature and the extrapolated value from Varshni's equation. A localization energy of 20 meV can then be deduced. In the case of the InGaN/GaN QW, the dependence of PL energy on temperature no longer follows the Varshni equation (figure 15(a)). Actually, excitons are deeply localized and some of them are still bound to potential fluctuations even at room temperature. The degree of localization can be assessed

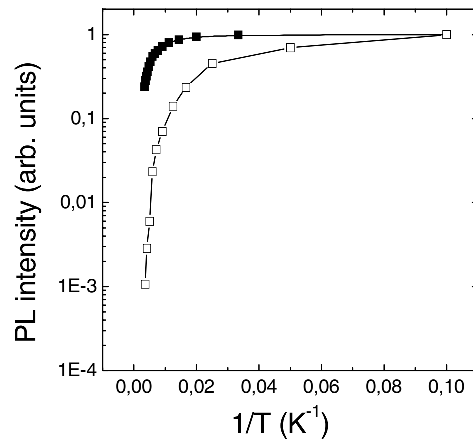

Figure 16. Arrhenius plots of the PL intensity of InGaN/GaN (closed squares) and GaN/AlGaN (open squares) QWs.

through the PL linewidth variation as a function of temperature. In figure 15(b) are reported the experimental PL linewidth of the GaN/AlGaN QW and the theoretical variation using a classical PL broadening equation (full line) involving exciton–phonon scattering [32]. Above 100 K, the data well agree with the theoretical curve because the regime of free excitons is reached. On the other hand, the PL linewidth of the InGaN/GaN QW exhibits a strong increase above 250 K compared to the case of GaN/AlGaN QW. This behaviour cannot be accounted for by exciton-phonon scattering but can be ascribed to thermally activated delocalization of excitons toward higher energy states. Actually, the PL energy variation between 10 and 300 K of the InGaN/GaN QW (figure 15(a)) is reduced because of the thermally activated higher energy states that participate in the PL spectrum at high temperature. One can therefore conclude from the comparison of GaN/AlGaN and InGaN/GaN QWs that in the latter the excitons are more deeply localized. Recombinations on dislocations are then hindered as for the case of GaN/AlN QDs. This explains why, despite the huge electric field that reduces the oscillator strength, the PL efficiency is still high. We have obtained for instance PL from 0.4 to 0.66 μm at room temperature [33]. As another illustration of the better PL efficiency of GaInN/GaN QWs over GaN/AlGaN QWs, we report Arrhenius plots in figure 16. The integrated PL intensity ratio between 10 and 300 K is about three orders of magnitude for GaN/AlGaN QWs whereas it is less than ten for GaInN/GaN QWs.

3.5. InGaN/GaN QW based LEDs

The InGaN/GaN QWs described above have been used in the active region of LEDs. The LED structure consists of a few microns of GaN:Si ($n > 1\times10^{18}$ cm^{-3}), an $In_{0.2}Ga_{0.8}N/GaN$ MQWs and a 0.2 μm thick GaN:Mg layer ($p \sim 3\times10^{17}$ cm^{-3}). LEDs are processed from square mesas of side 350 μm formed by reactive ion etching. The ohmic contacts to n- and p-GaN layers are respectively Ti/Al (150 Å/750 Å) and Ni/Au (50 Å/50 Å) semi-transparent current spreading layers plus a Ni/Au (200 Å/1000 Å) contact as top electrode. The electroluminescence (EL) is measured at room temperature under DC-biased conditions and collected from the surface side of the LEDs.

In figure 17 are reported the 300 K EL spectra of three different LEDs emitting in the blue, green and orange, respectively. The active regions contain three InGaN/GaN QWs with

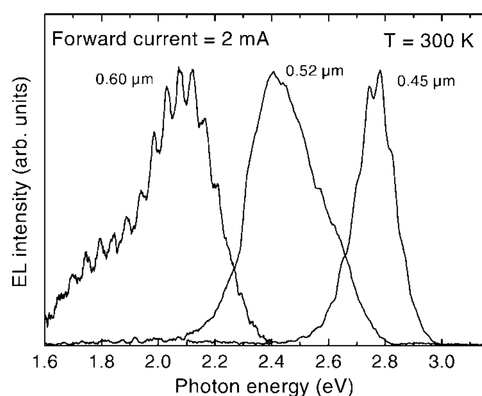

Figure 17. 300 K EL of InGaN/GaN based LEDs grown on sapphire substrate.

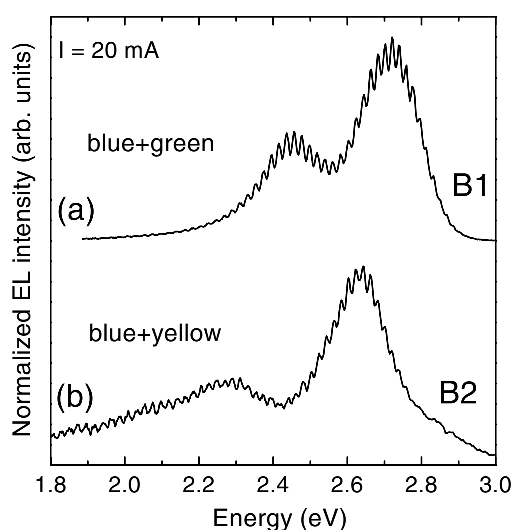

Figure 18. (a) EL spectrum of multicolour LED (B1) with two distinct peaks at 455 and 505 nm. (b) EL spectrum of white LED (B2) with two peaks at 470 and 550 nm.

thicknesses of 1.5, 3.5 and 5 nm, respectively. The maximum output power (0.3 mW at 20 mA) is obtained for blue LEDs. In that case, LEDs were grown on MOCVD GaN templates. The output power of LEDs entirely grown by MBE on sapphire or silicon substrates is lower (a few tens of μW).

Let us now consider InGaN/GaN LEDs with QWs of different thicknesses inside the GaN p–n junction. In the first LED, the active region consists of two 1.9 nm thick QWs followed by four others of thickness 3.9 nm. The EL spectrum (figure 18(a)) exhibits two distinct peaks, with maxima at 455 and 505 nm, that correspond to the emission of the two series of QWs. When the QW thicknesses are increased to 2.3 and 4.5 nm, the corresponding emissions are red-shifted toward wavelengths of 470 and 550 nm, respectively (figure 18(b)). The light emitted by such a LED is white for the naked eye. Actually, one can be more quantitative about the 'colour' of LEDs since any colour can be precisely defined by its chromaticity coordinates following the conventions of the Comité International de l'Eclairage (CIE) 1931.

The stacking of blue and yellow emitting QWs leads to nearly pure white light ($x = 0.29$, $y = 0.31$) when driving the p–n junction at 20 mA. The colour temperature (black body) is 8000 K, which is similar to hybrid nitride white LEDs (blue LEDs pumping phosphors). Note that the chromaticity coordinates of the present white LEDs depend slightly on the driving current. It must be pointed out that this technique is very flexible for the realization of white LEDs as the intensity ratio between the different colours can be adjusted by changing the number of each QW and also their arrangement in the p–n junction.

4. Conclusions

The huge polarization field that occurs in wurtzite phase nitride heterostructures has been exemplified through the optical properties of GaN/AlGaN QWs, InGaN/GaN QWs and GaN/AlN QDs. The giant QCSE involves a red-shift of the PL transition energy and a decrease of the oscillator strength. The latter effect may have a consequence of reducing the radiative efficiency, in particular in highly defective materials. However, the efficiency of GaN/AlN QDs and InGaN/GaN QWs is very high compared to GaN/AlGaN QWs. This is the consequence of the carrier localization either in true QDs or in potential wells formed by alloy composition fluctuation. Finally, we have shown that InGaN/GaN QWs can be used in LEDs for white light emission.

Acknowledgments

The authors would like to thank F Semond, S Laügt, P Vennéguès, M Leroux, A Bouilé, H Haas (CRHEA-CNRS) and C Pernot (CRHEA-CNRS/Picogiga), L Siozade and J Leymarie (LASMEA-CNRS, Clermont-Fd University), B Gil and P Lefebvre (GES-CNRS, Montpellier University), P Perlin (Unipress) and R Langer (Picogiga). This work is supported by BOQUANI and NANILUB contracts.

References

[1] Lefebvre P, Allègre J, Gil B, Kavokin A, Mathieu H, Morkoç H, Kim W, Salvador A and Botchkarev A 1998 *Phys. Rev.* B **57** R9447
[2] Grandjean N, Damilano B, Dalmasso S, Leroux M, Laügt M and Massies J 1999 *J. Appl. Phys.* **86** 3714
[3] Simon J, Langer R, Barski A and Pelekanos N T 2000 *Phys. Rev.* B **61** 7211
[4] Widmann F, Simon J, Daudin B, Feuillet G, Rouvière J L, Pelekanos N T and Fishman G 1998 *Phys. Rev.* B **58** R15 989
[5] Damilano B, Grandjean N, Semond F, Massies J and Leroux M 1999 *Appl. Phys. Lett.* **75** 962
[6] Damilano B, Grandjean N, Dalmasso S and Massies J 1999 *Appl. Phys. Lett.* **75** 3751
[7] Adelmann C, Simon J, Feuillet G, Pelekanos N T, Daudin B and Fishman G 2000 *Appl. Phys. Lett.* **76** 1570
[8] Grandjean N and Massies J 1997 *Appl. Phys. Lett.* **71** 1816
[9] Grandjean N and Massies J 1998 *Appl. Phys. Lett.* **73** 1260
[10] Kim W, Aktas Ö, Botcharev A E, Salvador A, Mohammad S N and Morkoç H 1996 *J. Appl. Phys.* **79** 7657
[11] Kamp M, Mayer M, Pelzmann A, Thies A, Chung H Y, Sternschulte H, Marti O and Ebeling K J 1996 *Mater. Res. Soc. Symp. Proc.* vol 395 (Pittsburgh, PA: Materials Research Society) p 135
[12] Kamp M, Mayer M, Pelzmann A, Thies A, Chung H Y, Sternschulte H, Marti O and Ebeling K J 1996 *Mater. Res. Soc. Symp. Proc.* vol 395 (Pittsburgh, PA: Materials Research Society) p 135
[13] Bernardini F, Fiorentini V and Vanderbilt D 1997 *Phys. Rev.* B **56** R10 024
[14] Im J S, Kollmer H, Off J, Sohmer A, Scholz F and Hangleiter A 1998 *Phys. Rev.* B **57** R9435
[15] Leroux M, Grandjean N, Laügt M, Massies J, Gil B, Lefebvre P and Bigenwald P 1998 *Phys. Rev.* B **58** R13 371
[16] Takeuchi T, Wetzel C, Yamaguchi S, Sakai H, Amano H, Akasaki I, Kaneko Y, Nakagawa S, Yamaoka Y and Yamada N 1998 *Appl. Phys. Lett.* **73** 1691
[17] Gérard J M, Cabrol O and Sermage B 1996 *Appl. Phys. Lett.* **68** 3123

[18] Narukawa Y, Kawakami Y, Funato M, Shizuo Fujita, Shigeo Fujita and Nakamura S 1997 *Appl. Phys. Lett.* **70** 981
[19] Semond F, Damilano B, Vézian S, Grandjean N, Leroux M and Massies J 1999 *Appl. Phys. Lett.* **74** 82
[20] Grandjean N, Damilano B, Dalmasso S, Leroux M, Laügt M and Massies J 1999 *Phys. Status Solidi* a **176** 219
[21] Massies J and Grandjean N 1993 *Phys. Rev. Lett.* **71** 1411
[22] Grandjean N, Massies J, Semond F, Karpov S Yu and Talalaev R A 1999 *Appl. Phys. Lett.* **74** 1854
[23] Della Sala F, Di Carlo A, Lugli P, Bernardini F, Fiorentini V, Scholz R and Jancu J M 1999 *Appl. Phys. Lett.* **74** 2002
[24] Nakamura S and Fasol G 1997 *The Blue Laser Diode* (Berlin: Springer)
[25] Guha S, Madhukar A and Rajkumar R C 1990 *Appl. Phys. Lett.* **57** 2110
[26] Snyder C W, Orr B G, Kessler D and Sander L M 1991 *Phys. Rev. Lett.* **66** 3032
[27] Grandjean N and Massies J 1998 *Appl. Phys. Lett.* **72** 1078
[28] Elsner J, Haugk M, Jungnickel G and Frauenheim Th 1998 *Solid State Commun.* **106** 739
[29] McCluskey M D, Van de Walle C G, Master C P, Romano L T and Johnson N M 1998 *Appl. Phys. Lett.* **72** 2725
[30] Bellaiche L, Mattila T, Wang L W, Wie S H and Zunger A 1999 *Appl. Phys. Lett.* **74** 1842
[31] Berkovicz E, Guershoni D, Bahir G, Lakin E, Shilo D, Zolotoyabko E, Abare A C, DenBaars S P and Coldren L A 2000 *Phys. Rev.* B **61** 10 994
[32] Kim D S, Shah J, Cunningham J E, Damen T C, Schäfer W, Hartmann M and Schmidt-Rink S 1992 *Phys. Rev. Lett.* **68** 1006
[33] Damilano B, Grandjean N, Massies J, Siozade L and Leymarie J 2000 *Appl. Phys. Lett.* **77** 1268